Surface & Coatings Technology 236 (2013) 246–251

Contents lists available at ScienceDirect

Surface & Coatings Technology

journal homepage: www.elsevier.com/locate/surfcoat

Evolution of structural and magnetic properties of Co–Fe based metallic glass thin films with thermal annealing

G. Pookat [a], H. Thomas [a], S. Thomas [a,1], S.H. Al-Harthi [b], L. Raghavan [a], I.A. Al-Omari [b], D. Sakthikumar [c], R.V. Ramanujan [d], M.R. Anantharaman [a,*]

[a] Department of Physics, Cochin University of Science & Technology, Cochin 682022, Kerala, India
[b] Department of Physics, Sultan Qaboos University, P.O. Box 36, Postal Code 123, Al Khod, Sultanate of Oman
[c] Graduate School of Interdisciplinary New Science, Toyo University, 350-8585, Japan
[d] School of Materials Science and Engineering, Nanyang Technological University, Singapore 639798, Singapore

ARTICLE INFO

Article history:
Received 3 April 2013
Accepted in revised form 30 September 2013
Available online 5 October 2013

Keywords:
CoFe based thin films
Thermal annealing
Nanocrystallization
Surface smoothening

ABSTRACT

Ultra thin films based on CoFe were prepared from a composite target employing thermal evaporation. The microstructure of the films was modified by thermal annealing. The relationship between microstructure and magnetic properties of the films was investigated using techniques like glancing angle X-ray diffraction (GXRD), transmission electron microscopy (TEM) and vibrating sample magnetometry (VSM). The GXRD and TEM investigations showed an onset of crystallization of CoFe at around 373 K. The magnetic softness of the films improved with thermal annealing but at higher annealing temperature it is found to be deteriorating. Annealing induced modification of surface morphology of the alloy thin films was probed by atomic force microscopy (AFM). Surface smoothening was observed with thermal annealing and the observed magnetic properties correlate well with surface modifications induced by thermal annealing.

1. Introduction

Amorphous and nanocrystalline magnetic alloys are in demand because of their excellent soft magnetic properties for applications in diverse fields, such as magneto-optic storage, magnetic shielding, and magnetic sensors [1–3]. Research interest in metallic glasses is growing over the last decade since the first discovery of amorphous alloys of Au–Si by Duwez et al. in 1959 [4]. The improvement in soft magnetic properties of the nanocrystalline alloys of Fe–Si–B–M (M = Cr, V, Mo, Nb, Ta, W) put forward by Yoshizawa et al. in 1988 [5] accelerated the growth of research in this area. Later, studies of the nanocrystalline families NANOPERM™ (Fe–Zr–B–Cu) [6] and HITPERM™ (Fe–Co–Zr–B–Cu) [7] shed further light on the origin of soft magnetic properties [8] and the amorphous nanocrystalline transformation [9,10]. Among them Co and Fe rich alloys are widely used in technological applications like sensors, actuators and magnetic recording heads [11,12] as they exhibit excellent magnetic properties like high Curie temperature, high permeability, low magnetic loss, low coercivity and high saturation magnetization [13–18]. Micro/Nano Electro Mechanical Systems (MEMS/NEMS) devices such as microactuators, sensors and micromotors can be realized with the use of both hard and soft magnetic materials. These electromagnetically actuated MEMS are more stable for large actuation gap and high force applications. The high magnetic moment of Co rich binary alloys makes it suitable for these applications [19,20]. Miniaturization of these materials are required for microelectronic applications, hence thin films of these alloys are of great importance [21]. The relatively high value of magnetostriction observed for CoFe thin films increases the levels of stress developed during the growth of CoFe films. The magnetic properties of such materials depend on various factors such as film thickness, crystal structure and size, composition and surface/interface roughness. Enhanced magnetic softness compared to their polycrystalline counterparts can be further improved, either by thermal annealing around the crystallization temperature or by electron/ion beam irradiation [5,22–25]. Annealing of amorphous alloy thin films enables the relaxation of the amorphous structure and initiates formation of a composite amorphous-crystalline, microstructure with crystal size of ~10 nm. Such a microstructure is expected to improve the soft magnetic properties. Several reports are there on thermally induced nanocrystallization in Co-based alloys [26–28]. Bordin et al. [29] reported the occurrence of superior soft magnetic properties with the evolution of nanocrystallites with heat treatment of $Co_{66}Fe_4Mo_2B_{11.5}Si_{16.5}$ amorphous ribbons well below their conventional crystallization temperature. Quintana et al. [26] reported the nanocrystallite formation below the conventional crystallization temperature in $Co_{66}Fe_4Mo_2Si_{16}B_{12}$. Buttino et al. [30] also reported improvements in soft magnetic properties of an amorphous alloy of composition $Co_{66}Fe_4Ni_1B_{14}Si_{15}$. The improvements were obtained by isothermal treatments below the conventional crystallization temperature.

* Corresponding author. Tel.: +91 4842577404; fax: +91 4842577057.
E-mail address: mraiyer@gmail.com (M.R. Anantharaman).
[1] Presently at: Institute of Physics, Chemnitz University of Technology, 09107 Chemnitz, Germany.

0257-8972/$ – see front matter © 2013 Elsevier B.V. All rights reserved.
http://dx.doi.org/10.1016/j.surfcoat.2013.09.055

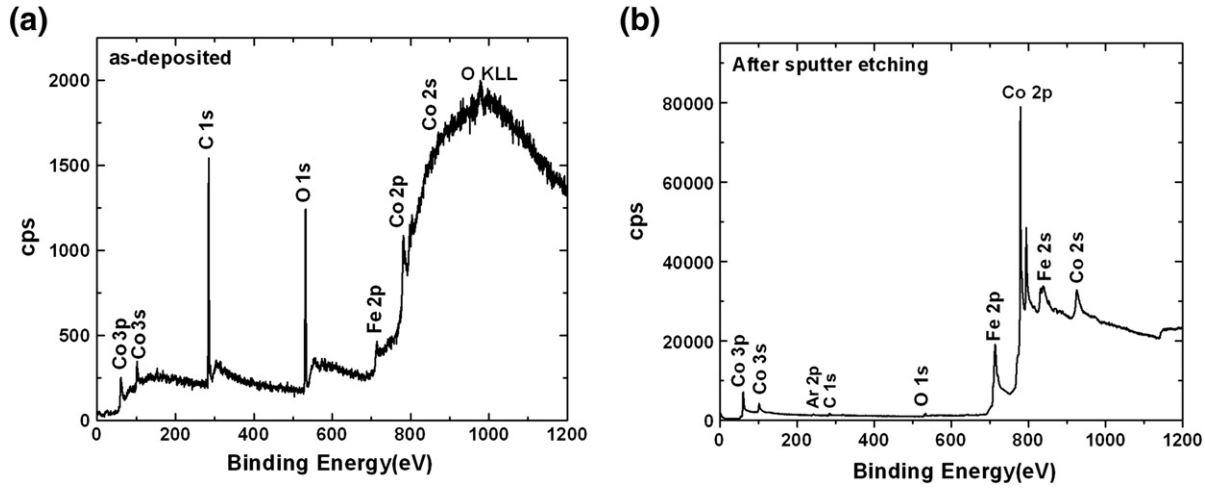

Fig. 1. XPS survey scan of (a) as-deposited film and (b) after sputter etching for 30 min using Ar^+.

Structural relaxation and crystallization during thermal annealing result in significant changes in magnetic properties. For example, nanocrystalline cobalt based alloys display superior magnetic softness compared to their amorphous counterparts [31,32]. The magnetic properties display a strong dependence on the nanocrystal size and distribution [33]. If the amorphous matrix is nonmagnetic, the behavior of the magnetic nanocrystals is governed by a single domain particle model; whereas the case of a magnetic matrix is more complicated. Detailed investigations of such nanocrystalline magnetic systems have resulted in useful developments for applications like soft underlayers for ultrahigh density computer disk drives and magnetic sensors [34–36].

The material under study here is CoFe based thin films where $Co_{75}Fe_{14}Ni_4Si_5B_2$ is used as target material. For the fabrication of amorphous alloy thin films one can employ processes like physical vapor deposition (PVD), chemical vapor deposition (CVD) or atomic layer deposition [37]. Here we have employed thermal evaporation which is a physical vapor deposition technique for the growth of thin film which is a cost effective technique and can be carried out in any common laboratory. It is to be noted that as-deposited films are amorphous in nature and in order to induce nanocrystallization thermal annealing is necessary. From a fundamental point of view investigation on the effects of thermal annealing assumes significance since the onset of nanocrystallization is very important and this determines its magnetic properties. Moreover, thermal annealing induces microstructural changes which in turn will have a bearing on the magnetic properties of the film. This is one of the primary objectives of the present investigation. Here we report the microstructural and magnetic evolution of CoFe based thin films on thermal annealing.

2. Experimental

Thin films based on CoFe were deposited on naturally oxidized silicon (100) substrates by thermal evaporation, using a composite target having the composition $Co_{75}Fe_{14}Ni_4Si_5B_2$. Film deposition was carried out at room temperature at a pressure of 1×10^{-6} Torr with the source to substrate distance of 11 cm. A set of samples were also deposited simultaneously onto NaCl substrates for TEM investigations. Differential thermal analysis (DTA) of the target material was carried out to find out the crystallization temperature of the material. On the basis of that study, as-deposited thin films were annealed at different temperatures (373 K, 473 K, 573 K and 673 K) for 1 h under high vacuum conditions (1×10^{-6} Torr) to initiate nanocrystallization in these films [22–24,38].

The thickness of the film was measured using Dektak 6M thickness profiler. GXRD study of the as-prepared and annealed films was performed using a Bruker Discover D-8 diffractometer with CuK_α ($\lambda = 1.54$ Å) radiation. X-ray photoelectron spectroscopy (XPS) study of the thin films was carried out using an Omicron Nanotechnology XPS system with a monochromatic Al K_α radiation ($h\nu = 1486.6$ eV), of source voltage 15 kV and emission current of 20 mA. All scans were

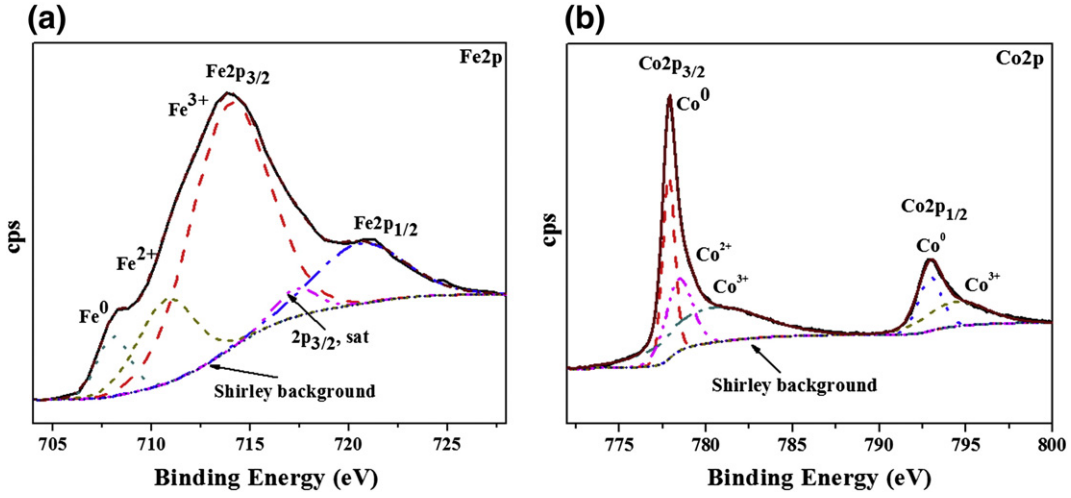

Fig. 2. High resolution XPS spectra of (a) Fe 2p, and (b) Co2p.

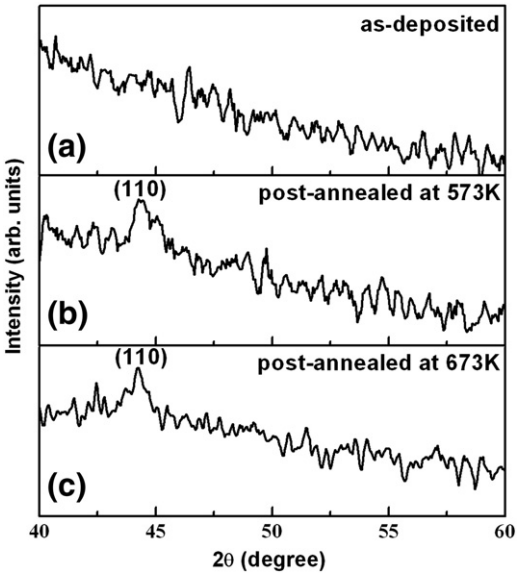

Fig. 3. GXRD patterns of (a) as-deposited, (b) 573 K, and (c) 673 K annealed CoFe based films.

carried out at a base pressure of 2×10^{-11} Torr. The wide scan was recorded with constant analyzer transmission energy of 50 eV, while the individual elemental peaks were recorded at analyzer pass energy of 20 eV. The obtained XPS spectra were deconvoluted using CasaXPS program (Casa Software Ltd., UK) [39] in which the background was simulated using Shirley function and the peaks were fitted using a Gaussian–Lorentzian function. The recorded spectra were corrected using the binding energy of aliphatic carbon at 285 eV and the accuracy of the measured binding energy values is estimated to be equal to ±0.2 eV. Room temperature magnetization measurements were carried out using a VSM (DMS 1660 VSM) with a magnetic field varying from −13 to +13 kOe. The microstructural evolution of the films was investigated by TEM (Joel JEM-2200 FS) operated at 200 kV. The surface morphology of the as-deposited and annealed CoFe based films was imaged using AFM multimode instrument, having higher resolution magnetic force microscopy tips (MESP-HR) (Bruker) with resonant frequency of 475 kHz. The magnetic force microscopy (MFM) imaging is carried out at a lift height of 10 nm, scan rate of 0.5 kHz and resolution of 512 pixels.

3. Results and discussion

The nominal thickness of the deposited thin films, as determined using a stylus profiler was found to be 40 nm. The wide scan XPS spectrum of the as-deposited film (Fig. 1(a)) shows the presence of cobalt and iron along with unavoidable surface contaminants like carbon and oxygen. XPS spectrum was also recorded after removing the surface oxide layer by Ar^+ sputtering (3 keV) for 30 min. The resultant spectrum shows that the film is rich in cobalt and iron along with traces of oxygen, carbon and argon (Fig. 1(b)). Argon is expected to be implanted in the films during the sputter etching process.

High resolution XPS spectra of the elemental components, Co and Fe acquired after removing the surface contaminants are shown in Fig. 2. Curve fitting of the experimental data presented in Fig. 2(a) revealed different components at binding energies 707.2 eV, 710.7 eV and 714.2 eV for Fe $2p_{3/2}$. These peaks represent the presence of Fe in different oxidation states, Fe^0, Fe^{2+} and Fe^{3+} [40]. The multiplet splitting of Fe 2p as well as a satellite peak of Fe $2p_{3/2}$ at around 717 eV

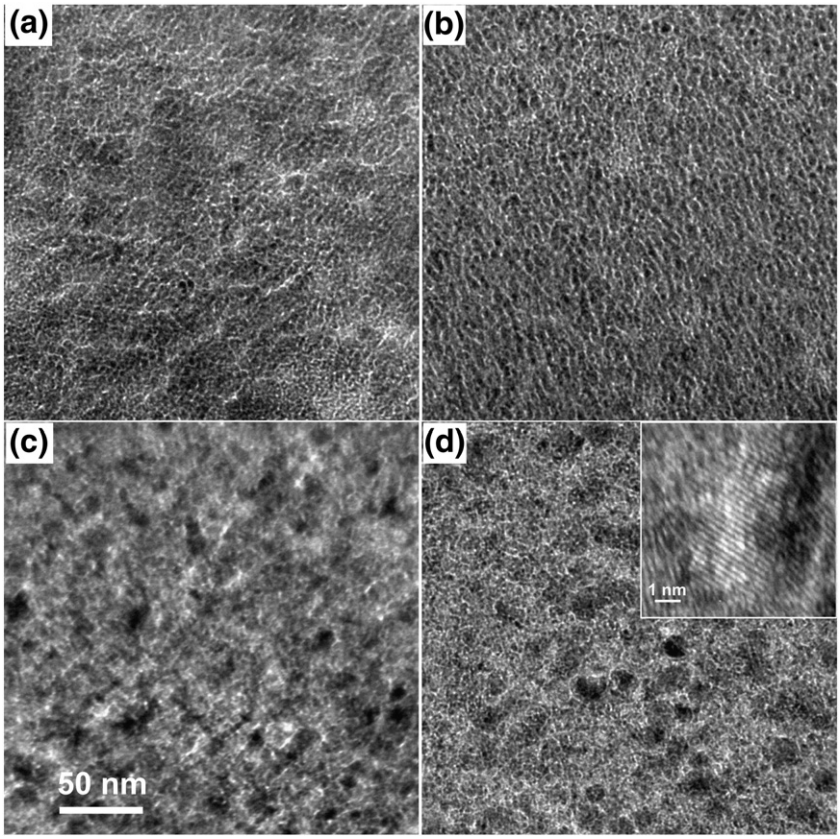

Fig. 4. TEM micrographs of thin films deposited on NaCl substrates and post-annealed at (a) 373 K, (b) 473 K, (c) 573 K, and (d) 673 K. HRTEM of 673 K annealed film is shown in the inset of (d).

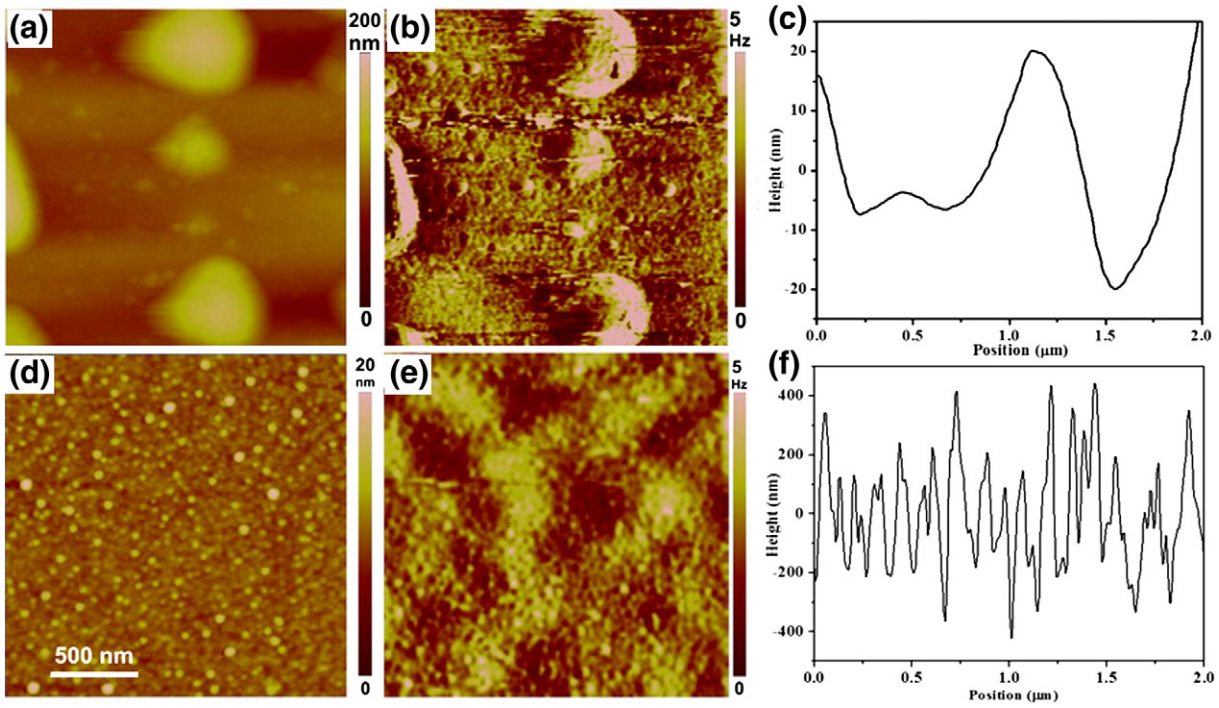

Fig. 5. (a) AFM & (b) MFM images and (c) line scan of as-deposited CoFe based thin films, (d) AFM & (e) MFM images and (f) line scan of 573 K annealed CoFe based thin films.

[40] was also observed. Corresponding Co 2p high resolution spectrum is shown in Fig. 2(b). Curve fitting to Co $2p_{3/2}$ line resulted in three components centered on 777, 778 and 780 eV, which corresponds to the presence of Co in the oxidation states Co^0, Co^{2+} and Co^{3+} respectively [41–43]. It is to be noted that the intensity of Fe $2p_{1/2}$ and Co $2p_{1/2}$ peaks was small for resolving all the three components that were observed for their corresponding $2p_{3/2}$ peaks.

High resolution XPS spectrum was also acquired in the energy range of 94–110 eV. However it was difficult to deconvolute the Si 2p and Co 3s lines because of their similar binding energies [44]. Quantification of the spectrum in Fig. 1(b) yielded the composition of the film as 76.81 wt.% of Co and 22.72 wt.% of Fe, along with traces of oxygen.

The XRD pattern of as-deposited and annealed films recorded in grazing incidence geometry is shown in Fig. 3. It is evident that the as-deposited film is amorphous and crystallization of the films is initiated at 573 K and 673 K which resulted in a diffraction peak centered around 44°, which can be assigned to the bcc CoFe (110) phase (JCPDS 49-1567) [45–47]. The amorphous nature was further confirmed using selective area diffraction pattern of the films (not presented). From the XPS analysis it is found that traces of oxygen are also present in the film along with Co and Fe. The presence of impurities like oxygen will increase the glass forming ability of metallic glasses which in turn can stabilize the amorphous phase in the as-prepared film [37].

The TEM micrographs for samples annealed at 373 K, 473 K, 573 K and 673 K are shown in Fig. 4. Nanocrystallites with average grain size of ~6 nm are clearly visible in the 473 K annealed film (Fig. 4b). Upon further heat treatment the average crystallite size increases in the 673 K annealed film (Fig. 4d). It is noteworthy that few crystallites of size ~19 nm were also observed in the bright field image of 673 K annealed samples along with ~15 nm.

HRTEM of the film annealed at 673 K is shown in the inset of Fig. 4(d). Well defined crystalline planes are visible in the micrograph. Planes observed in the HRTEM image have an average inter planar

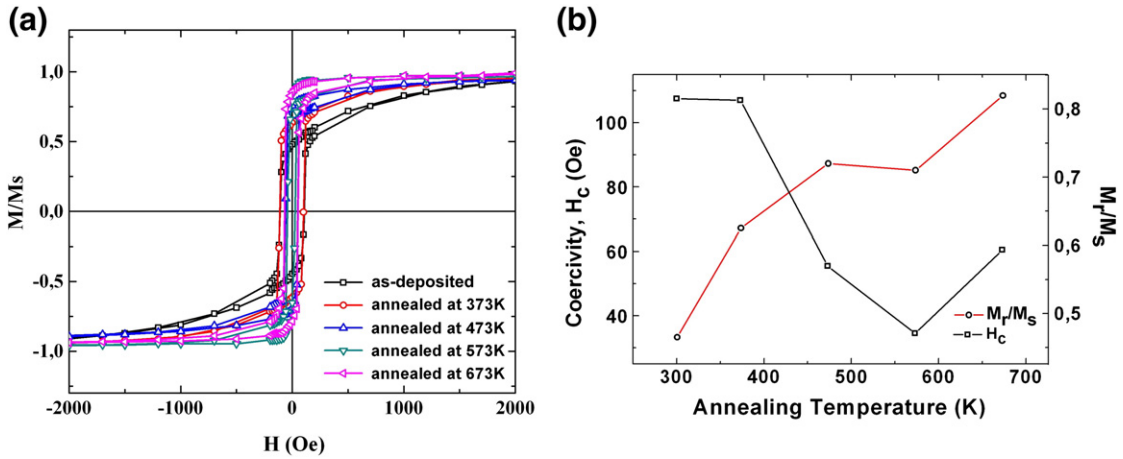

Fig. 6. (a) Room temperature hysteresis loops of as-deposited and annealed thin film samples and (b) coercivity and remanence dependence on annealing temperature. Solid line is a guide to the eye.

distance of 2.01 Å and the corresponding planes are identified as (110) planes of the crystalline CoFe phase [45–47], further supporting the results of GXRD measurements.

Atomic force microscopy was used to investigate surface evolution with thermal annealing. Fig. 5(a) shows $2 \times 2\,\mu m^2$ AFM image that was acquired from the as-deposited sample. Islands of lateral size around 500 nm with a height of about 40 nm are visible. Continuous and smooth morphology is observed in 573 K annealed samples with rms roughness of about 1.2 nm (Fig. 5(d)). Statistical analysis of the AFM images showed that the roughness of the films decreased gradually from 6.6 nm for as-deposited films to 1.1 nm for films annealed at 673 K. Volume and/or surface diffusion leads to the smoothening on thermal annealing [48]. AFM line scan depicted in Fig. 5(c) and (d) clearly demonstrates the changes in film morphology on thermal annealing.

The magnetic force microscopy image of the as-deposited CoFe based film acquired from $2 \times 2\,\mu m^2$ area is shown in Fig. 5(b). It can be seen that the image is dominated by topographical contrast. The MFM imaging was conducted for different tip heights and in all the images no meaningful magnetic images could be obtained. This is because of the absence of any stray magnetic fields along the out-of-plane direction. On the other hand, MFM images acquired from 573 K sample show distinctive features of 'dark' and 'bright' contrast suggesting magnetic stray fields emanating out from the film surface (Fig. 5(e)). For magnetic thin films with an easy magnetic direction along the film plane, the stray fields are expected to be from domain boundaries.

Fig. 6(a) depicts the magnetic hysteresis loop of the as-deposited film and the films annealed at various temperatures. There is a remarkable difference in the coercivity in as-deposited and annealed thin films. The variation of coercivity and remanence (M_r/M_s) with annealing temperature is depicted in Fig. 6(b) and it is evident that magnetic softening occurs at 573 K.

The gradual change in coercivity and remanence can be explained on the basis of microstructural and morphological changes in CoFe based thin films with thermal annealing. From TEM and AFM investigations it is seen that the as-deposited film is island-like, where the magnetization reversal occurs by rotation. Coercivity of 110 Oe is associated with the magneto-elastic anisotropies resulting from the rapid quenching of the films during film deposition [49]. Low remanence observed in the as-deposited film indicates that the demagnetization along the in-plane direction is due to the shape of the islands. On annealing at higher temperatures, stress relaxation occurs in films, at the same time crystallization and surface smoothening takes place. At 573 K, from the observed film morphology, it is expected that magnetization reversal is driven by a nucleation event followed by domain wall motion. This is a low energy process which is associated with low coercivity. At 673 K, the volume fraction of crystallites is expected to increase [50], which further impede domain wall motion, resulting in an increase in coercivity as well as remanence.

4. Conclusion

Thin films based on CoFe were prepared via thermal evaporation from a composite target of composition $Co_{75}Fe_{14}Ni_4Si_5B_2$. Post-annealing of these films resulted in nanocrystallites of CoFe in a residual amorphous matrix. Glancing angle X-ray diffraction of thin film samples annealed at 573 K and 673 K showed signatures of crystalline bcc CoFe phase. HRTEM studies further supported this finding. The as-deposited and post-annealed films were characterized using atomic force microscopy and it was found that a surface smoothening occurs in samples on thermal annealing. On annealing, crystallization together with surface smoothening influences the magnetization reversal. Magnetic measurements indicated that in as-deposited island-like films, magnetization reversal is via coherent rotation and the demagnetizing field significantly influences the reversal processes. Whereas, in films annealed at 573 K, the magnetization reversal is guided by a nucleation event followed by domain wall motion, resulting in low coercivity. Annealing at 673 K further resulted in an increase in coercivity as well as remanence.

Acknowledgment

GP acknowledges University Grants Commission (UGC), India for providing financial assistance in the form of RFSMS fellowship (No. F4-3/2006(BSR)/8-3/2007(BSR)). HT acknowledges UGC FDP for providing financial assistance. Dr. I. A. Al–Omari would like to thank Sultan Qaboos University for the support under the grant number IG/SCI/PHYS/12/02. LR & MRA are thankful to Inter University Accelerator Centre (IUAC), New Delhi for providing financial assistance in the form of UFUP project. MRA acknowledges Department of Science and Technology (DST)—Nanomission (No. SR/NM/NS-120/2010 (G)) and DST-DAAD (INT/FRG/DAAD/P-207/2011) for providing necessary facilities and financial assistance.

References

[1] R. Alben, J.J. Becker, M.C. Chi, J. Appl. Phys. 49 (1978) 1653.
[2] Y. Nishibe, H. Yamadera, N. Ohta, K. Tsukada, Y. Nonomura, Sensors Actuators A 82 (2000) 155.
[3] E. Hristoforou, J. Optoelectron. Adv. Mater. 4 (2) (2002) 245.
[4] W. Clement, R.H. Willens, P. Duwez, Nature 187 (1960) 869.
[5] Y. Yoshizawa, S. Oguma, K. Yamauchi, J. Appl. Phys. 64 (1988) 6044.
[6] A. Makino, K. Suzuki, A. InoueH, Y. Hirotsu, T. Masumoto, J. Magn. Magn. Mater. 133 (1994) 329.
[7] M.E. McHenry, D.E. Laughlin, Acta Mater. 48 (2000) 223–238.
[8] G. Herzer, Phys. Scr.T 49 (1993) 307.
[9] N. Lecaude, J.C. Perron, Mater. Sci. Eng. A 581–5 (1997) 226.
[10] L.K. Varga, E. Bakos, E. Kisdi-Koszo, E. Zsoldos, L.F. Kiss, J. Magn. Magn. Mater. 133 (1994) 280.
[11] R. Gupta, A. Khandelwal, R. Ansari, A. Gupta, K.G.M. Nair, Surf. Coat. Technol. 203 (2009) 2717.
[12] S. Mehrizi, M.H. Sohi, S.A.S. Ebrahimi, Surf. Coat. Technol. 205 (2011) 4757.
[13] L.H. Chen, T.J. Klemmer, K.A. Ellis, R.B. van Dover, S. Jin, J. Appl. Phys. 87 (2000) 5858.
[14] G. Rieger, G. Rupp, G. Gieres, R. Losehand, W. Hartung, W. Maass, W. Ocker, J. Appl. Phys. 91 (2002) 8447.
[15] A. Neudert, J. McCord, R. Schafer, L. Schultz, J. Appl. Phys. 95 (2002) 6595.
[16] H. Fujimori, S. Ohnuma, N. Kobayashi, T. Masumoto, J. Magn. Magn. Mater. 304 (2006) 32.
[17] R.H. Yu, S. Basu, Y. Zhang, J.Q. Xiao, J. Appl. Phys. 85 (1999) 6034.
[18] Lin Li, J. Appl. Phys. 79 (1996) 4578.
[19] B.Y. Yoo, S.C. Hernandez, D.-Y. Park, N.V. Myung, Electrochim. Acta 51 (2006) 6346–6352.
[20] M.R.J. Gibbs, E.W. Hill, P.J. Wright, J. Phys. D. Appl. Phys. 37 (2004) R237–R244.
[21] Saito N. Hasegawa, M. Saito, N. Kataoka, H. Fujimori, J. Mater. Eng. Perform. 2 (1993) 181.
[22] T. Hysen, S. Deepa, S. Saravanan, R.V. Ramanujan, D.K. Avasthi, P.A. Joy, S.D. Kulkarni, M.R. Anantharaman, J. Phys. D. Appl. Phys. 39 (2006) 1993.
[23] Senoy Thomas, S.H. Al-Harthi, R.V. Ramanujan, Zhao Bangchuan, Liu Yan, Wang Lan, M.R. Anantharaman, Appl. Phys. Lett. 94 (2009).
[24] Senoy Thomas, Hysen Thomas, D.K. Avasthi, A. Tripathi, R.V. Ramanujan, M.R. Anantharaman, J. Appl. Phys. 105 (2009).
[25] V.D. Das, Lakshmi, J. Phys. Rev. B 37 (1988).
[26] P. Quintana, E. Amano, R. Valenzuela, J.T.S. Irvine, J. Appl. Phys. 75 (1994) 6940.
[27] R.C. O'Handley, J. Mengusar, S.-W. Sun, Y. Hara, N.J. Grant, J. Appl. Phys. 57 (1985) 3563.
[28] I. Betancourt, M. Jim'enez, S. Aburto, V. Marquina, R. G'omez, M.L. Marquina, R. Ridaura, M. Miki, R. Valenzuela, J. Magn. Magn. Mater. 140–144 (1995) 459–460.
[29] G. Bordin, G. Buttino, A. Cecchetti, M. Poppi, J. Phys. D. Appl. Phys. 30 (1997) 2163.
[30] G. Buttino, A. Cecchetti, M. Poppi, J. Magn. Magn. Mater. 172 (1997) 147.
[31] C. Suryanarayana, Bull. Mater. Sci. 17 (1994) 307.
[32] H.F. Li, R.V. Ramanujan, Trans. Indian Inst. Met. 58 (2005) 965.
[33] M.J. Yongmei, Y.U. Wang, A. Kazaryan, Y. Wang, D.E. Laughlin, A.G. Khachaturyan, J. Appl. Phys. 92 (10) (2002) 6172.
[34] S. Sun, C.B. Murray, J. Appl. Phys. 85 (1999) 4325.
[35] V.F. Puntes, P. Gorostiza, D.M. Aruguete, N.G. Bastus, A.P. Alivisatos, Nat. Mater. 3 (2004) 263.
[36] S. Sun, C.B. Murray, D. Weller, L. Folks, A. Moser, Science 287 (2000) 1989.
[37] Hua Yan, Raissa Nathania Santoso, Yueyue Jiang, Meng Heng Liang, Zhong Chen, Thin Solid Films 520 (2012) 2356.
[38] S. Thomas, S.H. Al-Harthi, D. Sakthikumar, I.A. Al-Omari, R.V. Ramanujan, Y. Yoshida, M.R. Anantharaman, J. Phys. D Appl. Phys. 41 (2008) 155009.
[39] N. Fairley, http://www.casaxps.com 2005©Casa software Ltd.
[40] J.F. Moulder, W.F. Stickle, P.E. Sobol, K.D. Bomben, in: J. Chastain (Ed.), Handbook of X-ray Photoelectron Spectroscopy, MN: Perkin-Elmer Corporation, 1992, p. 222.
[41] Shijing Wang, Boping Zhang, Cuihua Zhao, Songjie Li, Meixia Zhang, Liping Yan, Appl. Surf. Sci. 257 (2011) 3358–3362.

[42] Mark C. Biesinger, Brad P. Payne, Andrew P. Grosvenor, Leo W.M. Lau, Andrea R. Gerson, Roger St.C. Smart, Appl. Surf. Sci. 257 (2011) 2717.
[43] S. Valeri, A. Borghi, G.C. Gazzadi, A. di Bona, Surf. Sci. 423 (1999) 346.
[44] M. Garcıa-Mendez, F.F. Castillon, G.A. Hirata, M.H. Farıas, G. Beamson, Appl. Surf. Sci. 161 (2000) 61.
[45] N.D. Ha, B.C. Park, C.G. Kim, C.O. Kim, Phys. Status Solidi (a) 201 (No.8) (2004) 1905–1908.
[46] X. Wang, F. Zheng, Z. Liu, X. Liu, D. Wei, F. Wei, J. Appl. Phys. 105 (2009) 07B714.
[47] W. Hua-Qiang, Y. Pin-Shi, Y.X. Hong, M.X. Dong, Y.G. Bao, W.W. Xian, J. Mater. Sci. 41 (2006) 6889.
[48] X. Junhua, Y. Lihua, K. Isao, J. Appl. Phys. 94 (2003) 6827.
[49] H. Giselher, J. Magn. Magn. Mater. 112 (1992) 258.
[50] C.S. Tsai, W.J. Yang, M.S. Leu, C.S. Lin, J. Appl. Phys. 70 (10) (1991) 5846–5848.